Ultrasensitive self-powered UV PDs via depolarization and heterojunction fields jointly enhanced carriers separation

Ying Zhang,[1] Jian Chen,[1] Qingfeng Zhang,[1,] Yinmei Lu,[1] Haitao Huang,[2] Yunbin He[1,*]

[1]Ministry of Education Key Laboratory of Green Preparation and Application for Functional Materials, Hubei Key Lab of Ferro & Piezoelectric Materials and Devices, Hubei Key Laboratory of Polymer Materials, School of Materials Science & Engineering, Hubei University, Wuhan 430062, China

[2]Department of Applied Physics, The Hong Kong Polytechnic University, Hong Kong, China

Abstract

In current semiconductor-based ultraviolet (UV) self-powered photodetectors (PDs), because the built-in electric field only exit in the space-charge region of p-n junction or schottky junction interfaces, the photo-generated carriers can't be separate efficiently and thus the photoelectric response is low. To solve this issue, in this study, we construct a new-type Pb,La(Zr,Ti)O_3 ferroelectrics/TiO_2 semiconductors heterojunction self-powered UV photodetector. By optimizing reasonably the TiO_2 layer number, the PDs with 2-layer TiO_2 thin film exhibit excellent self-powered ultraviolet photoelectric response performances with a large responsivity of 21 mA/W, high specific detectivity of 2.4×10^{11} Jones, and fast response speed (rise time of 2.4 ms, decay time of 3.2 ms) under a negative poling electric voltage. These values are far superior to those of all recently reported ferroelectric and semiconductor-based UV self-powered PDs. The huge improvement of the photoelectric response is

primarily because the depolarization field cause by the high remnant polarization of $Pb,La(Zr,Ti)O_3$ and the built-in electric field resulting from the heterojunction interfaces of the $Pb,La(Zr,Ti)O_3$ and the TiO_2 thin films enhance jointly the separation efficiency of photo-generated electron and holes. More interestingly, under weak-light illumination (0.18 mW/cm^2), the PDs exhibit a ultrahigh responsivity of 91.4 mA/W and large specific detectivity of 9.7×10^{11} Jones, which indicate its superior weak UV light detection ability. This work opens new avenue for designing and fabricating next-generation self-powered UV PDs by a simple, low-cost and easy to mass-produce way.

Keywords: $Pb,La(Zr,Ti)O_3$ ferroelectrics; TiO_2 semiconductors; Heterojunction; Self-powered; Ultraviolet photodetectors

1. INTRODUCTION

Ultraviolet (UV) photodetectors (PDs), which are prepared with wide band-gap materials (such as TiO_2, ZnO, SnO_2, Ga_2O_3 and GaN) [1-7], have been widely used in fire warning, wireless communication, missile tracking, environmental protection, remote control, and ozone hole detecting due to their superior photoelectric response properties and chemical thermal stability [8,9]. However, in order to convert UV light to electrical signal, these semiconductor-based UV PDs usually require an external driving force for the separation and transport of photo-generated carriers [10]. This causes a large amount of energy consumption and restricts the device miniaturization

and integration. Therefore, self-powered UV PDs drove by the built-in electric field and zero operating voltage have recently drawn more and more attention. At present, the built-in electric field is usually obtained by fabricating the junctions at the interface of two different materials, such as p-n junction between p- and n-type semiconductors, and schottky junction between semiconductors and metals. Nevertheless, these kinds of built-in electric fields exist only in the space-charge region of the junction interfaces, leading to low separation efficiency of photo-generated electrons and holes and thus weak photoelectric response. Therefore, the development of self-powered UV PDs fabricated by new materials is of great importance.

Different from conventional wide band-gap materials, ferroelectrics have large remnant polarization and thus high depolarization electric field throughout the whole bulk. This can cause efficient separation of photo-generated electron and hole even at zero bias and thus superior photoelectrical response. Besides, the wide band gap (> 3 eV) of ferroelectric materials is appropriate for preparing UV detectors. Based on above these advantages, ferroelectric based self-powered UV PDs have aroused extensive research interest [11-14]. Lately, we have fabricated Pb,La(Zr,Ti)O_3 ferroelectric based UV PDs, which exhibit the most superior photoelectric response performances in current ferroelectric based self-powered UV photodetectors attributed to large remnant polarization and thus high depolarized electric field of Pb,La(Zr,Ti)O_3 materials. However, due to the low carrier concentration of the ferroelectric materials, the photocurrent of this kind of photodetector is low, which

hence requires high-precision measurement systems to detect the signal. Therefore, there is a significant and urgent need to explore new strategy for high-performance ferroelectric based self-powered UV PDs.

Recently, ferroelectric/semiconductor heterostructures have drawn increasing attention because they takes the advantages of both the semiconductor and the ferroelectric properties and exhibited promising applications in photoelectric devices [15-17]. In heterojunction devices, electron and hole pairs are created inside both the semiconductor and ferroelectric layers and thus high carrier concentration can be obtained. More importantly, the depolarization field throughout the ferroelectrics and the built-in electric field resulting from the ferroelectric/semiconductor heterojunctions enhance jointly the separation efficiency of photo-generated carriers [15,18]. These two advantages can greatly cause the improvement of the photoelectric response for the photoelectric devices. For example, through the insertion of a $0.5Ba(Zr_{0.2}Ti_{0.8})O_3$-$0.5(Ba_{0.7}Ca_{0.3})TiO_3$ ferroelectric layer between n-Si and p-SnO_x, the values of short-circuit photocurrent density (J_{sc}), open-circuit voltage (V_{oc}), fill factor (FF) and power conversion efficiency (PCE) can improve from 12.6 $mAcm^{-2}$, 0.23 V, 27% and 8.3 % to 30.9 $mAcm^{-2}$, -2.0 V, 19% and 10.9 %, respectively [19]. However, until now, it has been still scarce to manipulate the ferroelectric effect for improving the photoelectric response of ferroelectric/semiconductor heterojunction self-powered UV PDs.

As stated above, we have already confirmed that $Pb,La(Zr,Ti)O_3$ ferroelectric thin films are promising materials for fabricating self-powered photoelectric devices

due to their large remnant polarization and hence high depolarization electric field, which can result in efficient and fast separation of the photo-generated electrons and holes [13,20-22]. Besides, TiO_2 semiconductor material has been regard as a good candidate for UV PDs due to its wide band-gap (~3.2 eV), high chemical and optical stability, non toxicity and low production cost. Based on above two factors, in this study, we design and fabricate Au/$Pb_{0.93}La_{0.07}(Zr_{0.2}Ti_{0.8})_{0.9825}O_3$ (PLZT)/TiO_2/FTO heterojunction self-powered UV PDs and discuss the internal mechanism of the influence of the TiO_2 layer numbers and the poling electric field on the photoelectric response of the device. At zero bias condition, the PD with 2-layers TiO_2 and -0.5 V poling electric voltage exhibits excellent photoelectric response performances with large responsivity of 21 mA/W, high detectivity of 2.4×10^{11} Jones, and fast response speed (rise time of 2.4 ms, decay time of 3.2 ms). These values are far superior to those of all recently reported self-powered UV detectors. This work provide a new way for designing and fabricating self-powered UV photodetectors with superior photoelectric response performances.

2. EXPERIMENTAL PROCEDURE

2.1. Fabrication of PLZT/TiO_2 heterojunction self-powered UV PDs

The TiO_2 precursor solutions were prepared via a sol-gel method. A certain amount of tetrabutyl titanate [$Ti(OC_4H_9)_4$] were added into the mixed solution of acetylacetone ($C_5H_8O_2$), glacial acetic acid (CH_3COOH) and ethylene glycol [$(CH_2OH)_2$] with stirring at room temperature for 2 h to obtain a clear and transparent

yellow solution, and then aged for 24 h to form a transparent sol. In the following, the sol was smeared on FTO substrates by spin-coating way at the rate of 3000 rpm for 30 s to ensure the uniformity and the above processes were respectively repeated 1, 2, 3 times to prepare TiO_2 thin film with multiple thickness. Then, those films were annealed at 600°C for 2 h in air for crystallization. After that, $Pb_{0.93}La_{0.07}(Zr_{0.2}Ti_{0.8})_{0.9825}O_3$ thin films were prepared on the TiO_2 films with different layer numbers by a spin-coating method, as reported in our previous work [20,21]. Finally, translucent square Au electrodes with a side length of 0.05 cm and a thickness of approximately 50 nm were deposited on the top surface of the PLZT thin films by thermal evaporation to fabricate the Au/PLZT/TiO_2/FTO heterojunction self-powered UV PDs.

2.2. The material and device characterization

The crystal structure of the PLZT/TiO_2 heterojunction thin films was characterized by X-ray diffraction (XRD, D8 Advance, Bruker, Germany). The surface and cross-sectional images were examined via field-emission scanning electron microscopy (FE-SEM, SIGMA 500, Germany). The optical properties were obtained using a UV-Vis-NIR spectrophotometer (UV-Vis-NIR, UV-3600 Plus, Shimadzu, Japan). Polarization-electric field (*P-E*) hysteresis loops were measured by a ferroelectric test system (Precision LC II; Radiant Technologies Inc, USA) at 100 Hz. The photoelectric response properties of the photodetector at different wavelengths and poling voltages were carried out by using a Keithley 2634 source meter, and during the measuring process, a 150 W low-pressure ultraviolet enhanced

xenon lamp was used as the light source, and monochromatic light was obtained through a grating spectrometer. The optical power was measured using a standard Si photodetector.

3. RESULTS AND DISCUSSION

Fig. 1 shows XRD patterns recorded in the 2θ range of 20° to 60° for PLZT/TiO_2 heterojunction thin films with different TiO_2 layer numbers. Obviously, all thin films have good crystal quality, no second or impurity phases are detected, and only the diffraction peaks from the PLZT and TiO_2 thin films are noted. Furthermore, It can be seen that there is a (101) reflection peak around 25.3° corresponding to anatase TiO_2 structure (PDF 71-1166) [23-26], and with increasing TiO_2 thickness, the intensity of the (101) diffraction peak gradually improves. All above these results confirm the successful preparation of PLZT/TiO_2 heterojunction thin films.

Fig. 2(a)-(c) display the FE-SEM surface morphology images of the PLZT/TiO_2 heterojunction thin films with different number of TiO_2 layers. It can be clearly observed that the thin films with 1-layer and 3-layer TiO_2 have many pores and the surface are uneven. Different from above these films, the films with 2-layer TiO_2 exhibit good uniformity, smooth and compactness, and no obvious macroscopic cracks are observed on the surface of the film, which is beneficial for obtaining superior photoelectric response. To investigate the interfaces of the PLZT/TiO_2 heterojunction thin films with different TiO_2 layer numbers, cross-sectional images are characterized and given in Fig. 2(d)-(f). As shown, for these three kinds of thin films,

the thickness of the TiO_2 layer are respectively 65 nm, 101 nm and 145 nm, and the PLZT layer thickness is about 300 nm. Besides, a well-interacted interface is formed between PLZT and TiO_2 layers, which is helpful to transfer carriers at the interface.

Fig. 3(a) shows the optical transmission spectra of the TiO_2 thin films, and PLZT/TiO_2 heterojunction thin films with different number of TiO_2 layers in the wavelength range of 295-800 nm. Clearly, all films are nearly transparent in the visible region (400-800 nm) and exhibit strong absorption for the UV light, which are favorable for fabricating UV PDs. In addition, as the TiO_2 thin film layer number increases, the transmittance of the TiO_2 thin films and PLZT/TiO_2 heterojunction thin film in the ultraviolet region gradually decreases, which means that the absorption ability of the thin films for the ultraviolet light is enhanced and thus more superior photoelectric response may be achieved. Here, the optical band gap (E_g) of the TiO_2 thin films and PLZT/TiO_2 heterojunction thin films can be determined by Tauc's Law [27,28],

$$(\alpha hv)^2 = A(hv - E_g) \quad (1)$$

where α, hv, and A are the absorption coefficient, photon energy, and constant, respectively. E_g can be calculated by extrapolating the linear portion of the $(\alpha hv)^2$ versus hv curve to zero, as displayed in the $(\alpha hv)^2$ vs. (hv) plots (Fig. 3(b)). Fig. 3(c) shows how the E_g of TiO_2 thin films and PLZT/TiO_2 heterojunction thin films varies with the TiO_2 layer number. Obviously, the E_g slightly decreases due to the influence of quantum size effect as the number of TiO_2 thin film layers increases [27]. Figure 3(d) illustrates room-temperature *P-E* hysteresis loops of the PLZT/TiO_2

heterojunction thin films. As seen, when the TiO_2 layer number is 1 and 2, square *P-E* loops, which is the typical character of ferroelectrics, are observed in the thin films, and the remnant polarization are respectively as high as 45.8 μC/cm^2 and 31.4 μC/cm^2, which is good for fabricating large depolarization electric field and thus the efficient separation of photo-generated electron-hole pairs. However, with increasing the TiO_2 layer number to 3, the square *P-E* loop is not obvious and the remnant polarization decreases to 14.8 μC/cm^2, which is mainly attributed to large leakage current caused by the TiO_2 semiconductor materials without spontaneous polarization.

In order to better discuss the origin of the photoelectric response of the PLZT/TiO_2 heterojunction PDs, we prepare TiO_2 UV PD with the Au/TiO_2/FTO structure, as shown in Fig. 4(a), and study the variation of the photocurrent of the devices with the TiO_2 layer number under intermittent UV illumination with 315 nm light at which the photocurrent is the largest, as given in Fig. 4(b)-(d). Clearly, the device with 2-layer TiO_2 exhibit the largest photocurrent (~ 90 nA), which is further higher than those with 1-and 3-layer TiO_2 because of its superior ultraviolet light absorption and photo-generated carriers separation ability. For the 1-layer TiO_2 thin film, as observed in Fig. 3(a), it has the weakest ultraviolet light absorption ability attributed to its thin thickness, and thus the concentration of the photo-generated carriers is low, which leads to small photocurrent. However, when the TiO_2 thickness is increased to 3 layer, although the concentration of the photo-generated carriers is high, the carrier recombination probability is improved, and thus the photocurrent decreases.

Fig. 5(a) presents the schematic diagram of the PLZT/TiO_2 heterojunction PDs with the Au/PLZT/TiO_2/FTO structure. The devices are poled by a Keithley 2634 source meter, and the negative poling direction is defined as the positive electric field applied to the FTO electrode. In order to more accurately investigate the effects of the poling voltages on the photoelectric response performances, after the devices are poled, a 5 min break is introduced before taking the measurement. Figure 5(b)-(d) illustrate current-time (*I*-*t*) curves of PLZT/TiO_2 heterojunction PDs with different number of TiO_2 layers under zero bias. Those devices are measured under the ultraviolet light with 340 nm wavelength at which their photocurrent is the largest. As seen, all devices exhibit superior self-powered performances and their photocurrent obviously improve with the increase of the poling electric field. In comparison with other devices, the PD with 2-layer TiO_2 has the maximum photocurrent of 180 nA under the poling electric voltage of -0.5 V, which is attributed to its good microstructure, superior ultraviolet light absorption ability and high photo-generated carriers separation efficiency. More interestingly, the photocurrent values of the heterojunction devices are further higher than those of TiO_2 PDs (Fig. 4) and PLZT PDs with the same layers which indicates the reasonability of this kind of device structure for fabricating self-powered PDs with high photoelectric response [22].

To further understand the internal mechanism of the poling voltage enhanced photoelectric responses in these Au/PLZT/TiO_2/FTO heterojunction devices, we provide schematic energy band diagrams of the devices at no poling and negative poling voltages under light illumination, as given in Fig. 6. It can be seen from Fig.

6(a) that without poling electric field, the dominant driving force for photo-generated carriers in Au/PLZT/TiO_2/FTO devices is the heterojunction field (E_j) formed at the interface between PLZT and TiO_2 thin films, which is attributed to the difference of the work function for these two kind of thin films [29,30]. When a negative electric field is applied, a depolarization electric field (E_{dp}) is generated inside the PLZT thin film and its direction is the same as that of the E_j. As a result, at this point, the total built-in electric field (E_{tot}) is equal to $E_j + E_{dp}$, which is more beneficial for the separation of the photo-generated electron and hole pairs and the improvement of the carriers mobility, and thus the photocurrent obviously increases with the application of the negative poling voltage.

For photodetectors, the spectral responsivity (R) and specific detectivity (D^*) are two critical parameters to evaluate the performance of the devices. The responsivity R, which represents the efficiency of a detector responding to optical signals, is calculated as follow [31-33]:

$$R_\lambda = \frac{I_{light} - I_{dark}}{P_\lambda S} \tag{2}$$

where I_{light} is the photocurrent, I_{dark} is the dark current, P_λ is the light intensity at each wavelength, and S is the effective illumination area ($S = 0.05 \times 0.05$ cm^2 in this work). D^* reflects the ability of a detector to detect signals from the noise environment and can be defined as Eq. (2) [34],

$$D^* = \frac{R_\lambda \sqrt{S}}{\sqrt{2eI_{dark}}} \tag{3}$$

where e is the charge of an electron ($e = 1.602 \times 10^{-19}$ C). Fig. 7(a)-(c) give the R and

*D** of the PDs with different number of TiO_2 layers at the negative poling voltages. In those devices, because the device with 2-layer TiO_2 has the largest photocurrent of 180 nA, as observed in Fig. 5, it exhibit the highest responsivity of 21 mA/W and largest detectivity of 2.4×10^{11} Jones. In order to characterize the detection ability of the PDs on the light signal with different intensities, Fig. 8 gives the dependence of the photoelectric response on the light power. As seen, with decreasing light intensity, although the photocurrent of all PDs reduce due to the decrease of the concentration of photo-generated electron and holes, the *R* and *D** gradually increase [18,34-36]. Especially, under the weak-ultraviolet light illumination (0.18 mW/cm^2, 340 nm), the Au/PLZT/TiO_2/FTO heterojunction PDs with 2-layer TiO_2 exhibit an ultrahigh *R* of 91.4 mA/W and *D** of 9.7×10^{11} Jones, respectively, which indicates that the PDs can be applicable in a wide field.

Besides *R* and *D**, another important parameter for characterizing the photoelectric response performance of photodetectors is the response speed. The rise time is the time required to convert a UV signal into an electrical signal, while the decay time represents the time required for the current to be restored to its original state, and thus they are both expected to be as fast as possible [22]. The rise time (t_r) and the decay time (t_d) are respectively the time of the photocurrent increasing from 10% to 90% as the light turns on, and the photocurrent decreasing from 90% to 10% as the light turn off [10,34]. Fig. 9(a)-(c) display respective the *I-t* curve of the Au/PLZT/TiO_2/FTO heterojunction PDs with different number of TiO_2 layers under a single UV illumination period. As observed, the device with 2-layer TiO_2 exhibits

the faster response speed with a rise/decay time of 2.4/3.2 ms, which is resulted from its good surface morphology, large depolarization electric field and thus the most superior photo-generated carries separation ability.

The key parameters of the PLZT/TiO_2 heterojunction self-powered UV PDs with different TiO_2 layer numbers, are summarized in Table 1. Obviously, the PD with 2-layer TiO_2 exhibits the most superior photoelectric response characteristics with a fast response and recover time of 2.4/3.2 ms, large R of 21 mA/W and high D^* of 2.4 × 10^{11} Jones. In addition, we compare the photoelectric response performances of recently reported ferroelectric and semiconductor-based self-powered UV PDs, as presented in Table [10,11,13,18,32,37-41]. Clearly, the self-powered UV PD with the Au/PLZT/TiO_2/FTO heterostructure obtained in this work exhibits the largest responsivity, highest specific detectivity, and fastest response speed among those self-powered UV PDs. This occurs primarily because the collaborative enhancement effect of the built-in electric field resulting from the heterojunction interfaces of the PLZT and the TiO_2 thin films and the depolarization field caused by the high remnant polarization of PLZT thin films can lead to photo-generated electron-hole pairs separation more effective and faster. This work provides an effective and simple way that can be scaled up for designing and fabricating self-powered UV PDs with excellent photoelectric response performances.

4. CONCLUSIONS

In summary, we have successfully prepared PLZT/TiO_2 heterojunction thin films

with different TiO_2 layer numbers through a facile spin-coating method and based on these films, constructed self-powered UV PDs with Au/PLZT/TiO_2/FTO structure. In comparison with PLZT and TiO_2-based PDs, because of the increase of the photo-generated carriers and the total built-in electric field, the photoelectric response performances of the PLZT/TiO_2 heterojunction PDs obviously improve. In addition, we have also found that the TiO_2 layer number has obvious effective on the photoelectric response properties of the PDs. When the TiO_2 layer number is 2, the PD exhibits superior microstructure, UV light absorption properties and photo-generated carriers separation efficiency, and thus the best self-powered UV light detection ability with a high responsivity of 21 mA/W, large specific detectivity of 2.4×10^{11} Jones, and fast response speed (rise time of 2.4 ms and decay time of 3.2 ms). Furthermore, under weak-light illumination (0.18 mW/cm^2), the R and D^* can be respectively as high as 91.4 mA/W and 9.7×10^{11} Jones, which greatly broaden the applicable range of this kind of self-powered UV PDs. The ferroelectrics/ semiconductors heterojunction strategy proposed in this work provide references for the designing and fabrication next-generation high-performances self-powered UV photodetectors.

ACKNOWLEDGMENTS

This work was supported by the National Key R&D Program of China (Grant No. 2019YFB1503500), the National Natural Science Foundation of China (Grant Nos. 11774082, 51872079), the Natural Science Foundation of Hubei Province (Grant Nos.

2019CFA006, 2019CFA055), the Program for Science and Technology Innovation Team in Colleges of Hubei Province (T201901), the Research Grants Council of the Hong Kong Special Administrative Region, China (Project No. PolyU152140/19E), and Shenzhen Science and Technology Innovation Committee (SGDX2019081623240364).

REFERENCES

[1] J. Xing, H. Wei, E.-J. Guo, F. Yang, Highly sensitive fast-response UV photodetectors based on epitaxial TiO_2 films, J. Phys. D: Appl. Phys. 44 (2011) 375104.

[2] D.B. Patela, K.R. Chauhana, W.-H. Parka, H.-S. Kima, J. Kima, J.-H. Yun, Tunable TiO_2 films for high-performing transparent Schottky photodetector, Mater. Sci. Semicond. Process. 61 (2017) 45-49.

[3] L.W. Ji, S.M. Peng, Y.K. Su, S.J. Young, C.Z. Wu, W.B. Cheng, Ultraviolet photodetectors based on selectively grown ZnO nanorod arrays, Appl. Phys. Lett. 94 (2009) 203106.

[4] K. Shen, X. Li, H. Xu, M. Wang, X. Dai, J. Guo, T. Zhang, S. Li, G. Zou, K.-L. Choy, I.P. Parkin, Z. Guo, H. Liu, J. Wu, Enhanced performance of ZnO nanoparticle decorated all-inorganic $CsPbBr_3$ quantum dot photodetectors, J. Mater. Chem. A 7 (2019) 6134-6142.

[5] M. Patel, H.-S. Kim, J. Kim, All transparent metal oxide ultraviolet photodetector, Adv. Electron. Mater. 1 (2015) 1500232.

[6] H. Chen, L. Hu, X. Fang, L. Wu, General fabrication of monolayer SnO_2 nanonets for high-performance ultraviolet photodetectors, Adv. Funct. Mater. 22 (2012) 1229-1235.

[7] A. Gundimeda, S. Krishna, N. Aggarwal, A. Sharma, N.D. Sharma, K.K. Maurya, S. Husale, G. Gupta, Fabrication of non-polar GaN based highly responsive and fast UV photodetector, Appl. Phys. Lett. 110 (2017) 103507.

[8] M. Huang, M. Wang, C. Chen, Z. Ma, X. Li, J. Han, Y. Wu, Broadband black-phosphorus photodetectors with high responsivity, Adv. Mater. 28 (2016) 3481-3485.

[9] Z.L. Wang, Self-powered nanosensors and nanosystems, Adv. Mater. 24 (2012) 280-285.

[10] D. Chen, Y. Xin, B. Lu, X. Pan, J. Huang, H. He, Z. Ye, Self-powered ultraviolet photovoltaic photodetector based on graphene/ZnO heterostructure, Appl. Surf. Sci. 529 (2020) 147087.

[11] N. Ma, K. Zhang, Y. Yang, Photovoltaic-pyroelectric coupled effect induced electricity for self-powered photodetector system, Adv. Mater. 29 (2017) 1703694.

[12] J. Qi, N. Ma, Y. Yang, Photovoltaic-pyroelectric coupled effect based nanogenerators for self-powered photodetector system, Adv. Mater. Interfaces 5 (2018) 1701189.

[13] J. Chen, A.S. Priya, D. You, W. Pei, Q. Zhang, Y. Lu, M. Li, J. Guo, Y. He, Self-driven ultraviolet photodetectors based on ferroelectric depolarization field

and interfacial potential, Sens. Actuators, A 315 (2020) 112267.

[14] A.B. Swain, M. Rath, P.P. Biswas, M.S. R. Rao, P. Murugavel, Polarization controlled photovoltaic and self-powered photodetector characteristics in Pb-free ferroelectric thin film, APL Mater. 7 (2019) 011106.

[15] D. Cao, C. Wang, F. Zheng, W. Dong, L. Fang, M. Shen, High-efficiency ferroelectric-film solar cells with an n-type Cu_2O cathode buffer layer, Nano Lett. 12 (2012) 2803-2809.

[16] J.P.B. Silva, K.C. Sekhar, F. Cortés-Juan, R.F. Negrea, A.C. Kuncser, J.P. Connolly, C. Ghica, J.A. Moreira, Ferroelectric photovoltaic characteristics of pulsed laser deposited $0.5Ba(Zr_{0.2}Ti_{0.8})O_3$-$0.5(Ba_{0.7}Ca_{0.3})TiO_3$/ZnO heterostructures, Sol. Energy 167 (2018) 18-23.

[17] J. Zhang, C. Yang, S. Wu, Y. Liu, M. Zhang, H. Chen, W. Zhang, Y. Li, Tuning two-dimensional electron gas of ferroelectric/GaN heterostructures by ferroelectric polarization, Semicond. Sci. Technol. 25 (2010) 035011.

[18] J. Chen, D. You, Y. Zhang, T. Zhang, C. Yao, Q. Zhang, M. Li, Y. Lu, Y. He, Highly sensitive and tunable self-powered UV photodetectors driven jointly by p-n junction and ferroelectric polarization, ACS Appl. Mater. Interfaces 12 (2020) 53957-53965.

[19] J.P.B. Silva, E.M.F. Vieira, J.M.B. Silva, K. Gwozdz, F.G. Figueiras, K. Veltruská, V. Matolín, M.C. Istrate, C. Ghica, K.C. Sekhar, A.L. Kholkin, L.M. Goncalves, A. Chahboun, M. Pereira, Perovskite ferroelectric thin film as an efficient interface to enhance the photovoltaic characteristics of Si/SnO_x

heterojunctions, J. Mater. Chem. A 8 (2020) 11314-11326.

[20] G. Chen, K. Zou, Y. Yu, Y. Zhang, Q. Zhang, Y. Lu, Y. He, Effects of the film thickness and poling electric field on photovoltaic performances of (Pb,La)(Zr,Ti)O_3 ferroelectric thin film-based devices, Ceram. Int. 46 (2020) 4148-4153.

[21] G. Chen, Y. Zhang, Q. Zhang, Y. Lu, Y. He, Superior ferroelectric photovoltaic properties in Fe-modified (Pb,La)(Zr,Ti)O_3 thin film by improving the remnant polarization and reducing the band gap, Ceram. Int. 46 (2020) 15061-15065.

[22] Y. Zhang, J. Chen, Y. Cai, Q. Zhang, Y. Lu, H. Huang, Y. He, Depolarization electric field and poling voltage modulated Pb,La(Zr,Ti)O_3-based self-powered ultraviolet photodetectors, J. Am. Ceram. Soc. 104 (2021) 928-935.

[23] A. Yu, S. Zhan, L. Qiu, X. Wang, H. Yang, Y. Li, Ultraviolet detector with ultrahigh responsivity based on Anatase TiO_2 nanotubes array modified with (001) exposed nanofacets, Vacuum 151 (2018) 237-242.

[24] H. Zhang, S. Ruan, C. Feng, B. Xu, W. Chen, W. Dong, Photoelectric Properties of TiO_2-ZrO_2 Thin Films Prepared by Sol-Gel Method, J. Nanosci. Nanotechnol. 11 (2011) 10003-10006.

[25] M.N. Tahir, B. Oschmann, D. Buchholz, X.W. Dou, I. Lieberwirth, M. Panthöfer, W. Tremel, R. Zentel, S. Passerini, Extraordinary performance of carbon-coated anatase TiO_2 as sodium-ion anode, Adv. Energy Mater. 64 (2016) 1501489.

[26] H. Fang, C. Zheng, L. Wu, Y. Li, J. Cai, M. Hu, X. Fang, R. Ma, Q. Wang, H. Wang, Solution-processed self-powered transparent ultraviolet photodetectors

with ultrafast response speed for high-performance communication system, Adv. Funct. Mater. 29 (2019) 1809013.

[27] M. Zhang, M. Xu, M. Li, Q. Zhang, Y. Lu, J. Chen, M. Li, J. Dai, C. Chen, Y. He, SnO_2 epitaxial films with varying thickness on c-sapphire: Structure evolution and optical band gap modulation, Appl. Surf. Sci. 423 (2017) 611-618.

[28] J. He, L. Sun, S. Chen, Y. Chen, P. Yang, J. Chu, Composition dependence of structure and optical properties of $Cu_2ZnSn(S,Se)_4$ solid solutions: an experimental study, J. Alloys Compd. 511 (2012) 129-132.

[29] J. Wang, R.G. Wilks, R. Félix, X.X. Liao, A. Grigoriev, M. Bär, The $Pb(Zr_{0.2},Ti_{0.8})O_3$/ZnO/GaN ferroelectric-semiconductor heterostructure: insight into the interfacial energy level alignments, Adv. Mater. Interfaces 7 (2020) 2000201.

[30] A. Perez-Tomas, E. Chikoidze, Y. Dumont, M.R. Jennings, S.O. Russell, P. Vales-Castro, G. Catalan, M. Lira-Cantú, C. Ton-That, F.H. Teherani, V.E. Sandana, P. Bove, D.J. Rogers, Giant bulk photovoltaic effect in solar cell architectures with ultrawide bandgap Ga_2O_3 transparent conducting electrodes, Mater. Today Energy 14 (2019) 100350.

[31] K.W. Liu, M. Sakurai, M. Aono, D.Z. Shen, Ultrahigh-gain single SnO_2 microrod photoconductor on flexible substrate with fast recovery speed, Adv. Funct. Mater. 25 (2015) 3157-3163.

[32] L. Zheng, P. Yu, K. Hu, F. Teng, H. Chen, X. Fang, Scalable production, self-powered TiO_2 nanowells/organic hybrids UV Photodetectors with Tunable

Performances, ACS Appl. Mater. Interfaces 8 (2016) 33924-33932.

[33] D. Han, K.Liu, Q. Hou, X. Chen, J. Yang, B. Li, Z. Zhang, L. Liu, D. Shen, Self-powered solar-blind $ZnGa_2O_4$ UV photodetector with ultra-fast response speed, Sens. Actuators, A 315 (2020) 112354.

[34] H. Geng, H. Xiao, L. Guan, H. Zhong, C. Hu, Z. Shi, Y. Guo, Visible or near-infrared light self-powered photodetectors based on transparent ferroelectric ceramics, ACS Appl. Mater. Interfaces 12 (2020) 33950-33959.

[35] J. Qi, N. Ma, X. Ma, R. Adelung, Y. Yang, Enhanced photocurrent in $BiFeO_3$ materials by coupling temperature and thermo-phototronic effects for self-powered ultraviolet photodetector system, ACS Appl. Mater. Interfaces 10 (2018) 13712-13719.

[36] Y. Li, Z. Shi, W. Liang, L. Wang, S. Li, F. Zhang, Z. Ma, Y. Wang, Y. Tian, D. Wu, Highly stable and spectrum-selective ultraviolet photodetectors based on lead-free copper-based perovskites, Mater. Horiz. 7 (2020) 530-540.

[37] J. Xu, W. Yang, H. Chen, L. Zheng, M. Hu, Y. Li, X. Fang, Efficiency enhancement of TiO_2 self-powered UV photodetectors using transparent Ag nanowires electrode, J. Mater. Chem. C 6 (2018) 3334-3340.

[38] P.K. Shanmuga, L. Kola, S. Pal, P. Biswas, P. Murugavel, Physical vapor deposited organic ferroelectric diisopropylammonium bromide film and its self-powered photodetector characteristics, RSC Adv. 10 (2020) 25773.

[39] J. Chen, J. Xu, S. Shi, R. Cao, D. Liu, Y. Bu, P. Yang, J. Xu, X. Zhang, L. Li, Novel self-powered photodetector with binary photoswitching based on

SnS_x/TiO_2 heterojunctions, ACS Appl. Mater. Interfaces 12 (2020) 23145-23154.

[40] L. Zheng, F. Teng, Z. Zhang, B. Zhao, X. Fang, Large scale, highly efficient and self-powered UV photodetectors enabled by all-solid-state n-TiO_2 nanowells/p-NiO mesoporous nanosheets heterojunction, J. Mater. Chem. C 4 (2016) 10032-10039.

[41] Y. Wang, C. Wu, D. Guo, P. Li, S. Wang, A. Liu, C. Li, F. Wu, W. Tang, All-oxide NiO/Ga_2O_3 p-n junction for self-powered UV photodetector, ACS Appl. Electron. Mater. 2 (2020) 2032-2038.

Figure captions:

Fig. 1. XRD patterns of PLZT/TiO_2 heterojunction thin films with different TiO_2 layer numbers.

Fig. 2. (a)-(c) FE-SEM images and (d)-(f) FE-SEM cross-sectional images of the PLZT/TiO_2 heterojunction thin films with different TiO_2 layer numbers.

Fig. 3. (a) Optical transmittance spectra; (b) $(\alpha hv)^2$ versus hv plots; (c) band gap values of TiO_2 thin films and PLZT/TiO_2 heterojunction thin films; and (d) *P-E* loops of PLZT/TiO_2 heterojunction thin films with different TiO_2 layer numbers.

Fig. 4. (a) Schematic structure diagram of TiO_2 thin film UV photodetectors. (b)-(d) Time-dependent photocurrent response of TiO_2 photodetectors with various TiO_2 layer numbers: (b) TiO_2-1 layers; (c) TiO_2-2 layers; (d) TiO_2-3 layers.

Fig. 5. (a) Schematic structure diagram of PLZT/TiO_2 heterojunction UV photodetectors. (b)-(d) Time-dependent photocurrent response of PLZT/TiO_2 heterojunction photodetectors with various TiO_2 layer numbers: (b) PLZT/TiO_2-1 layers; (c) PLZT/TiO_2-2 layers; (d) PLZT/TiO_2-3 layers at the negative poling voltages under switched-on/off UV light illumination.

Fig. 6. The schematic energy band diagrams of the photodetector with Au/PLZT/TiO_2/FTO structure under different polarization states: (a) without poling;

(b) negative poling.

Fig. 7. The responsivity and specific detectivity of PLZT/TiO_2 heterojunction photodetectors with various TiO_2 layer numbers: (a) PLZT/TiO_2-1 layers; (b) PLZT/TiO_2-2 layers; (c) PLZT/TiO_2-3 layers at the negative poling voltages.

Fig. 8. *I-t* curves of PLZT/TiO_2 heterojunction photodetectors with different TiO_2 layer numbers at the negative poling voltages and 340 nm light irradiation with various intensities: (a) PLZT/TiO_2-1 layers; (b) PLZT/TiO_2-2 layers; (c) PLZT/TiO_2-3 layers. Light power density-dependent *R*, and *D** with the TiO_2 layer number: (d) PLZT/TiO_2-1 layers; (e) PLZT/TiO_2-2 layers; (f) PLZT/TiO_2-3 layers.

Fig. 9. Single-cycle, time-dependent photocurrent of PLZT/TiO_2 heterojunction photodetectors with various TiO_2 layer numbers: (a) PLZT/TiO_2-1 layers; (b) PLZT/TiO_2-2 layers; (c) PLZT/TiO_2-3 layers at the negative poling voltages and under switched-on/off UV light illumination.

Fig. 1.

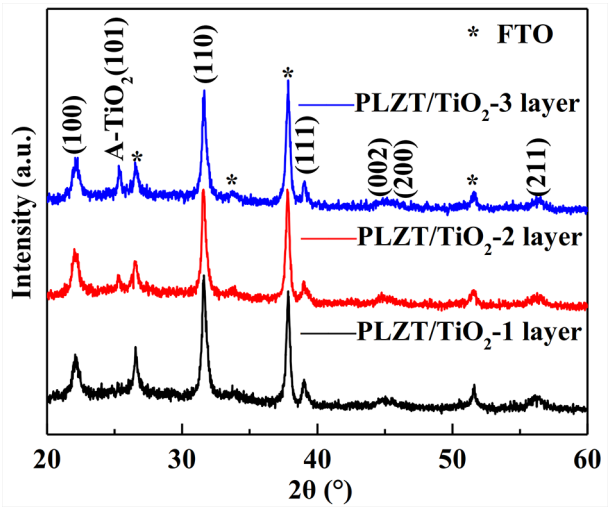
* FTO
(100)
A-TiO2(101)
(110)
(111)
(002)
(200)
(211)
PLZT/TiO2-3 layer
PLZT/TiO2-2 layer
PLZT/TiO2-1 layer
Intensity (a.u.)
20
30
40
50
60
2θ (°)

Fig. 2.

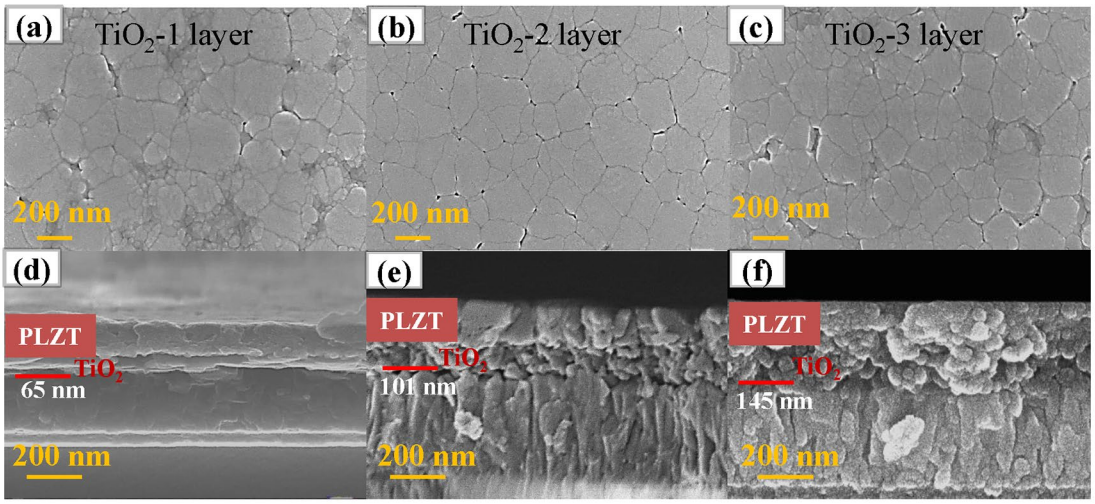
(a)
TiO2-1 layer
200 nm
(b)
TiO2-2 layer
200 nm
(c)
TiO2-3 layer
200 nm
(d)
PLZT
TiO2
65 nm
200 nm
(e)
PLZT
TiO2
101 nm
200 nm
(f)
PLZT
TiO2
145 nm
200 nm

Fig. 3.

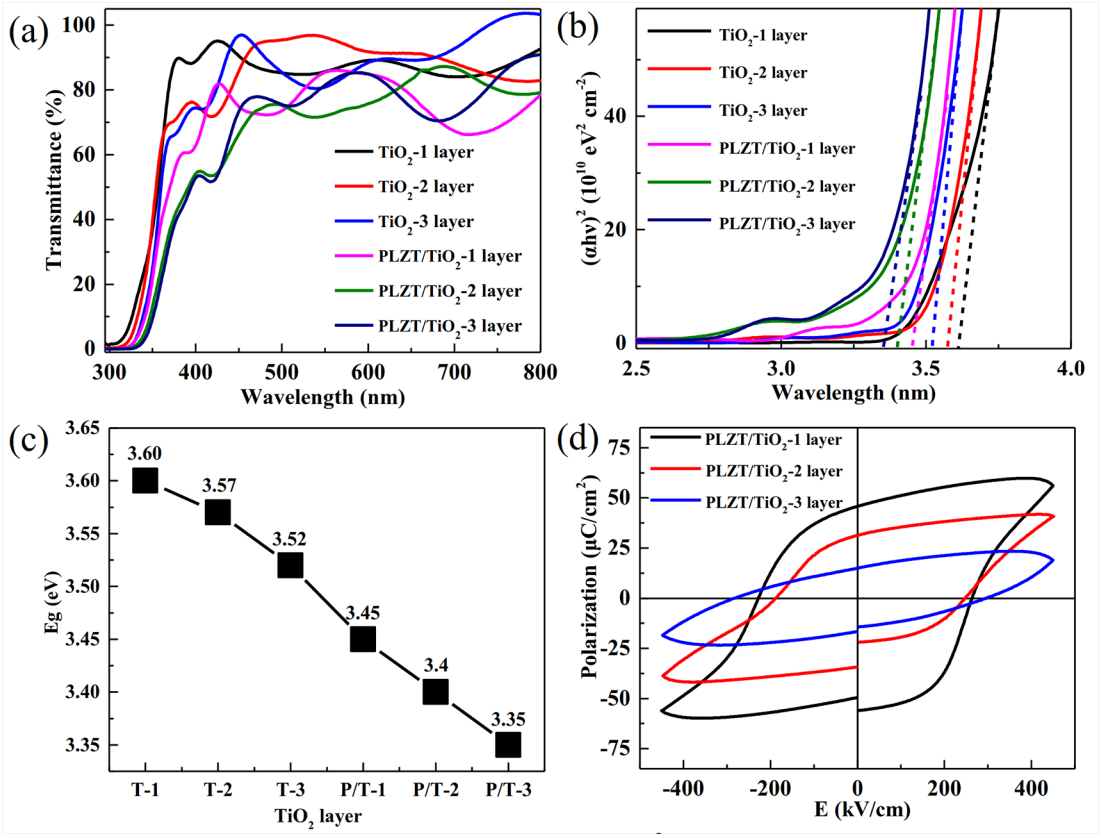
(a)
Transmittance (%)
Wavelength (nm)
TiO2-1 layer
TiO2-2 layer
TiO2-3 layer
PLZT/TiO2-1 layer
PLZT/TiO2-2 layer
PLZT/TiO2-3 layer
(b)
(αhν)2 (10^10 eV2 cm-2)
Wavelength (nm)
(c)
Eg (eV)
3.60
3.57
3.52
3.45
3.4
3.35
T-1
T-2
T-3
P/T-1
P/T-2
P/T-3
TiO2 layer
(d)
Polarization (μC/cm2)
E (kV/cm)

Fig. 4.

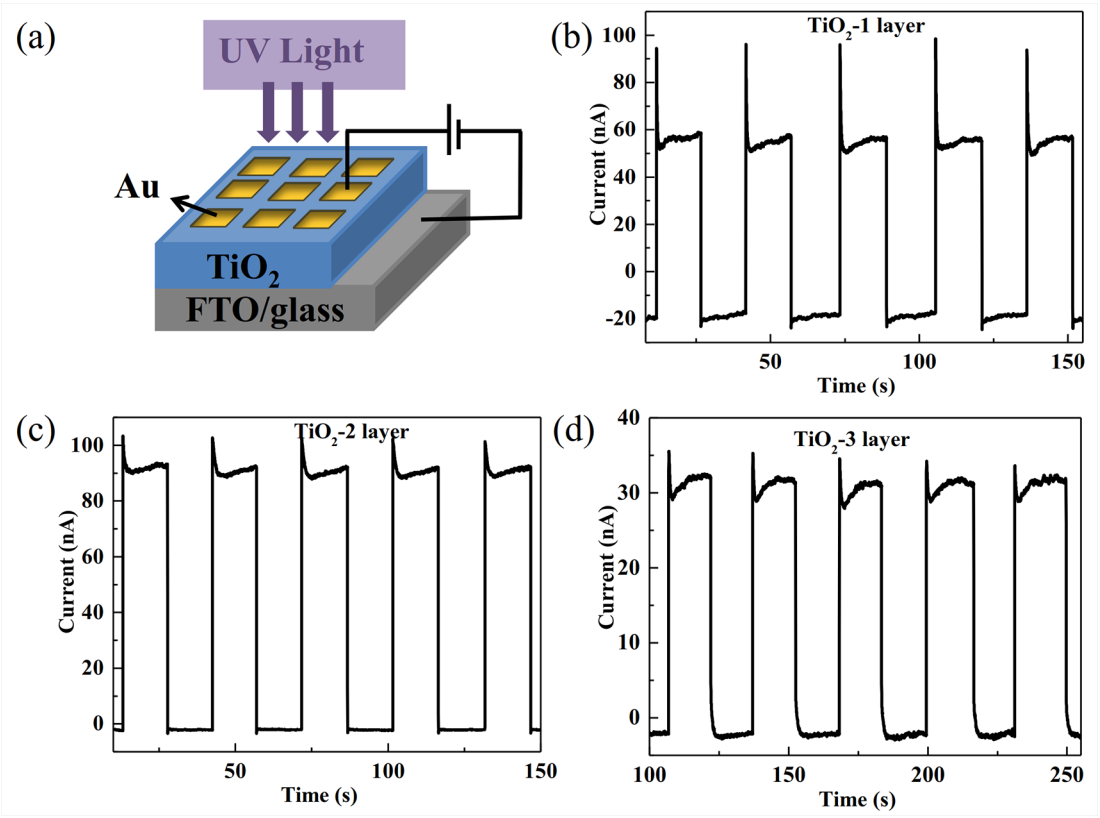
(a)
UV Light
Au
TiO2
FTO/glass
(b)
TiO2-1 layer
Current (nA)
Time (s)
(c)
TiO2-2 layer
Current (nA)
Time (s)
(d)
TiO2-3 layer
Current (nA)
Time (s)

Fig. 5.

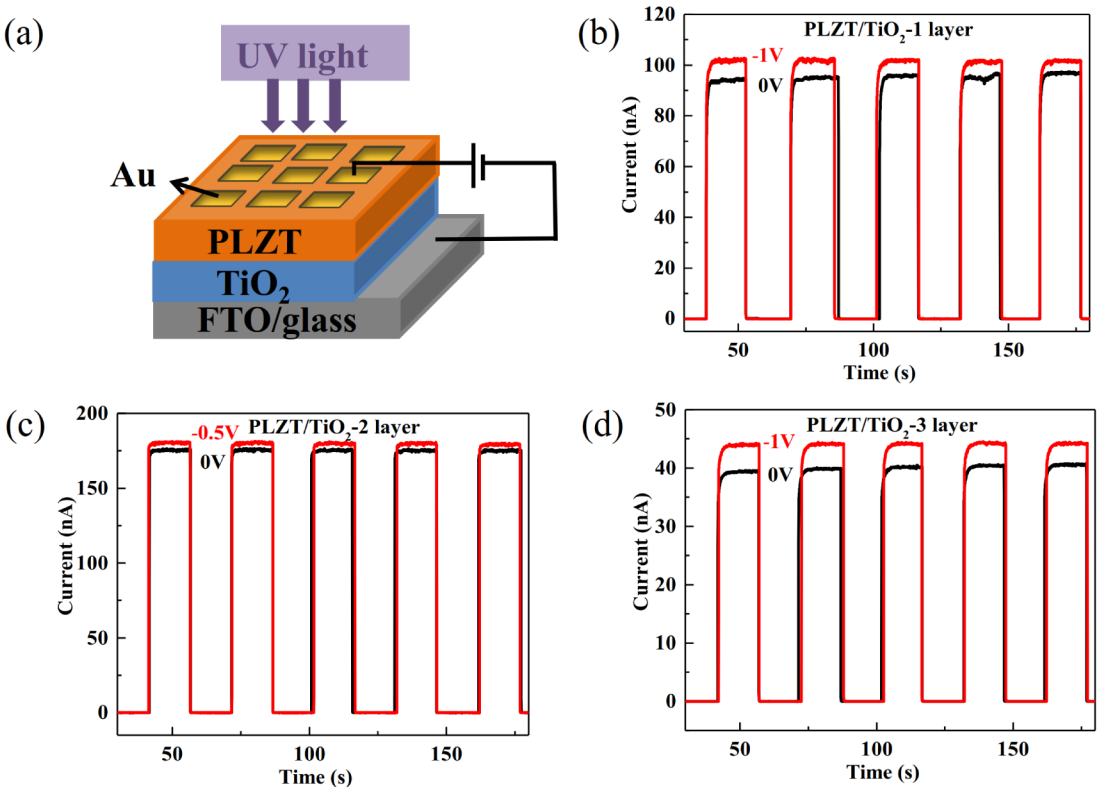
(a)
UV light
Au
PLZT
TiO2
FTO/glass
(b)
PLZT/TiO2-1 layer
-1V
0V
Current (nA)
Time (s)
(c)
-0.5V
PLZT/TiO2-2 layer
0V
Current (nA)
Time (s)
(d)
PLZT/TiO2-3 layer
-1V
0V
Current (nA)
Time (s)

Fig. 6.

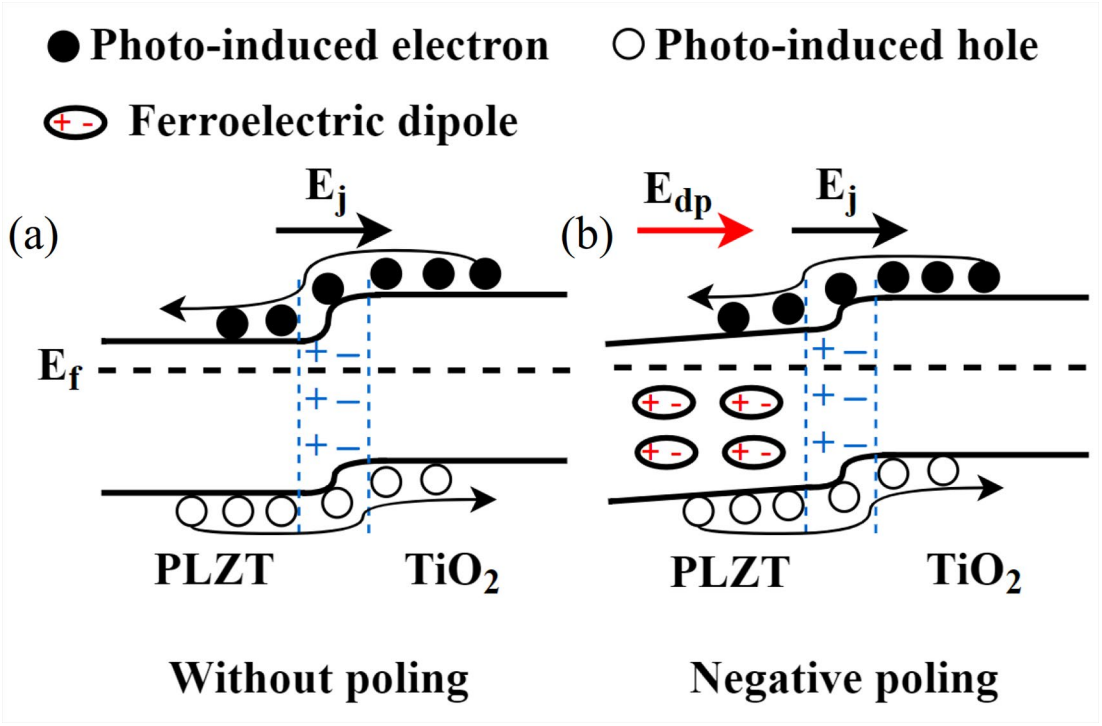
Photo-induced electron
Photo-induced hole
Ferroelectric dipole
(a)
(b)
E_j
E_{dp}
E_j
E_f
PLZT
TiO_2
PLZT
TiO_2
Without poling
Negative poling

Fig. 7.

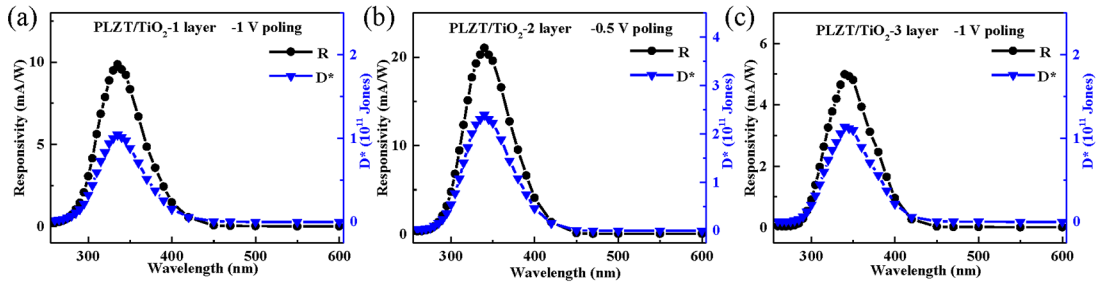
(a)
PLZT/TiO2-1 layer -1 V poling
R
D*
Responsivity (mA/W)
D* (10^11 Jones)
Wavelength (nm)
(b)
PLZT/TiO2-2 layer -0.5 V poling
R
D*
Responsivity (mA/W)
D* (10^11 Jones)
Wavelength (nm)
(c)
PLZT/TiO2-3 layer -1 V poling
R
D*
Responsivity (mA/W)
D* (10^11 Jones)
Wavelength (nm)

Fig. 8.

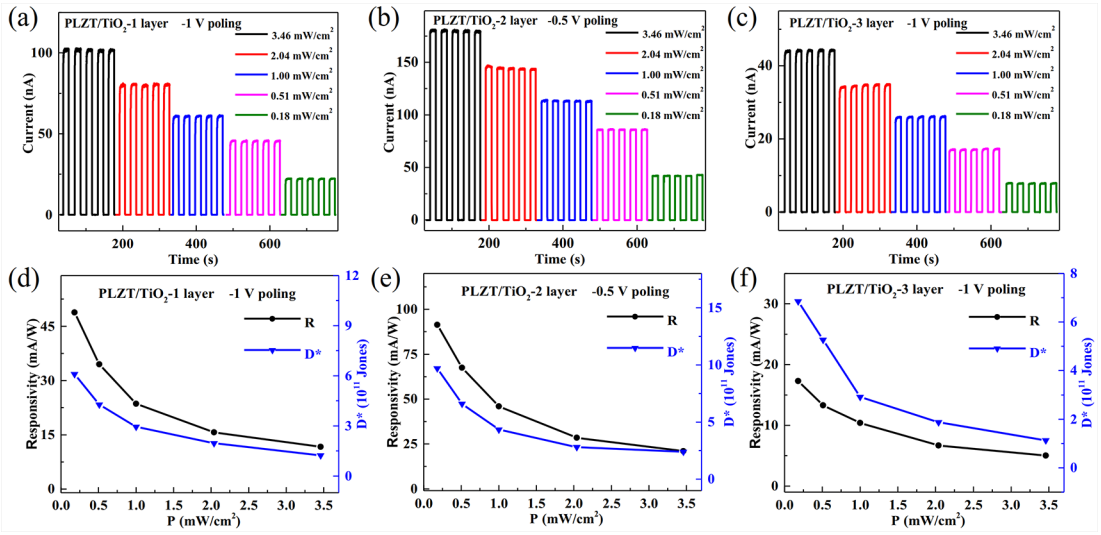
(a)
PLZT/TiO2-1 layer -1 V poling
3.46 mW/cm2
2.04 mW/cm2
1.00 mW/cm2
0.51 mW/cm2
0.18 mW/cm2
Current (nA)
Time (s)
(b)
PLZT/TiO2-2 layer -0.5 V poling
(c)
PLZT/TiO2-3 layer -1 V poling
(d)
PLZT/TiO2-1 layer -1 V poling
R
D*
Responsivity (mA/W)
D* (10^11 Jones)
P (mW/cm2)
(e)
PLZT/TiO2-2 layer -0.5 V poling
(f)
PLZT/TiO2-3 layer -1 V poling

Fig. 9.

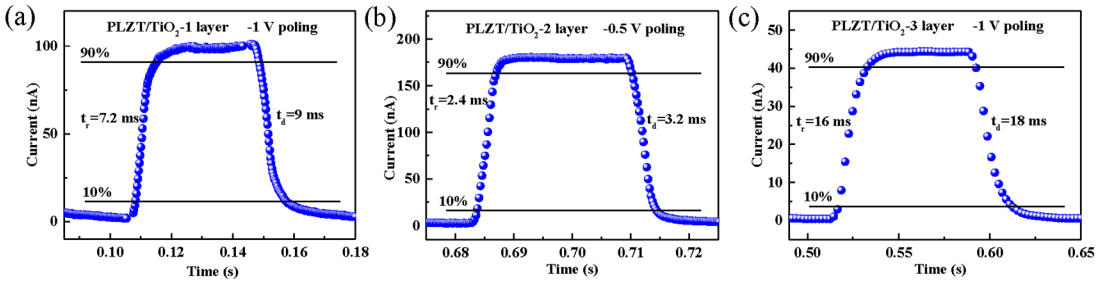
(a)
PLZT/TiO2-1 layer -1 V poling
90%
10%
tr=7.2 ms
td=9 ms
Current (nA)
Time (s)
(b)
PLZT/TiO2-2 layer -0.5 V poling
90%
10%
tr=2.4 ms
td=3.2 ms
Current (nA)
Time (s)
(c)
PLZT/TiO2-3 layer -1 V poling
90%
10%
tr=16 ms
td=18 ms
Current (nA)
Time (s)